Available online at www.sciencedirect.com
ScienceDirect
Journal of Photochemistry and Photobiology A: Chemistry 188 (2007) 112–119
Journal of Photochemistry and Photobiology A:Chemistry
www.elsevier.com/locate/jphotochem

Optimization of CdS/TiO_2 nano-bulk composite photocatalysts for hydrogen production from Na_2S/Na_2SO_3 aqueous electrolyte solution under visible light ($\lambda \geq 420$ nm)

Jum Suk Jang, Sang Min Ji, Sang Won Bae, Hyo Chang Son, Jae Sung Lee *

Eco-friendly Catalysis and Energy Laboratory (NRL), Department of Chemical Engineering and School of Environmental Science and Engineering, Pohang University of Science and Technology (POSTECH), San 31 Hyoja-dong, Pohang 790-784, Republic of Korea

Received 7 June 2006; received in revised form 20 October 2006; accepted 29 November 2006
Available online 1 December 2006

Abstract

A CdS/TiO_2 nano-bulk composite photocatalyst consisting of bulky CdS with a high crystallinity decorated with nanosized TiO_2 particles was fabricated by precipitation method and sol–gel synthesis. This configuration of the composite photocatalyst exhibited a very high rate of hydrogen production under visible light irradiation ($\lambda \geq 420$ nm) from water containing sulfide and sulfite as hole scavengers. In this work, we investigated the physicochemical properties of CdS(bulk)/TiO_2 composite photocatalysts and optimized their preparation conditions for the high photocatalytic activity of hydrogen production from water containing Na_2S and Na_2SO_3 as a sacrificial reagents under visible light irradiation.

Keywords: CdS; TiO_2; Nano-bulk composite (NBC); H_2 evolution

1. Introduction

Photocatalysts could convert solar energy into chemical energy by producing hydrogen gas from hydrogen-containing compounds. Thus, hydrogen production by use of semiconductor photocatalysts has recently received much attention with this view. Since visible light accounts for the largest portion (ca. 46%) of the solar spectrum, visible light-driven photocatalysts that could produce hydrogen from water splitting or aqueous electrolyte solutions under solar light have been actively sought [1–5]. Among them, composite systems made of more than two semiconductor components considered a promising method to develop a high efficiency photocatalyst working under visible light because they can compensate for the disadvantages of the individual component, and induce a synergistic effect, such as an efficient charge separation and improvement of photostability [6,7]. The CdS is a fascinating material having an ideal band gap energy and band positions for hydrogen production from water under visible light [8]. But, CdS is very unstable against photocorrosion in aqueous solutions under irradiation unless the solutions contain sacrificial agents, such as S^{2-} and/or SO_3^{2-} [9,10]. These sacrificial agents scavenge holes in the valence band of CdS before they attack CdS itself. In spite of this limitation, CdS possesses higher activity for hydrogen production than that of oxide materials in the presence of sacrificial reagents under visible light. To overcome this stability problem and improve the photoactivity, CdS has been combined with electron transfer medium, such as ZnO, TiO_2 and $LaMnO_3$ or intercalated into the layered compound [11–14]. These materials effectively accept electrons photogenerated from the conduction band of CdS to their own conduction band and improve the charge separation of photogenerated electrons and holes. As a new composite system, we already reported CdS(bulk)/TiO_2 nano-bulk composite photocatalysis [15]. This configuration of the composite photocatalyst exhibited a very high rate of hydrogen production under visible light ($\lambda \geq 420$ nm) from aqueous solution containing sulfide and sulfite as hole scavengers.

In this paper, we investigated the correlation between the photocatalytic activity and preparation conditions of CdS(bulk)/TiO_2 composite photocatalysts.

* Corresponding author. Fax: +82 54 279 5528.
E-mail address: jlee@postech.ac.kr (J.S. Lee).

1010-6030/$ – see front matter © 2006 Elsevier B.V. All rights reserved.
doi:10.1016/j.jphotochem.2006.11.027

2. Experimental

2.1. Preparation of bulk CdS photocatalysts

The CdS photocatalysts were prepared by a precipitation method. A stoichiometric amount of Na_2S aqueous solution was mixed drop-by-drop with $Cd(NO_3)_2$ dissolved in isopropyl alcohol. Precipitated powder was filtered and dried. The dried powder was calcined at 873–1073 K for 1–3 h under He flow (40 cc/min, 29.78 μmol s^{-1}) to increase the crystallinity of CdS. As a reference material, we used a commercial CdS powder (Aldrich).

2.2. Preparation of CdS(bulk)/TiO_2 composite photocatalysts

To fabricate CdS/TiO_2 nanocomposite photocatalysts, bulky CdS calcined at 1073 K for 1 h under He flow was stirred in isopropyl alcohol and TTiP (tetra-titanium isopropoxide) (in a mole ratio of CdS to TiO_2 from 1 to 0–4) and H_2O was added drop-by-drop. The prepared composite powder was filtered and dried again. The dried powder was calcined at 573–773 K for 1–3 h under air flow to increase the crystallinity of TiO_2 in CdS–TiO_2 composite photocatalysts.

2.3. Characterization

The crystalline phases of the products were determined by powder X-ray diffraction (XRD) on a diffractometer (Mac Science Co., M18XHF) with monochromatic Cu Kα radiation at 40 kV and 200 mA. The optical property was analyzed by UV–vis diffuse reflectance spectrometer (Shimadzu, UV 2401). The morphology of photocatalysts was investigated by field emission scanning electron microscopy (SEM, Hitachi, S-4200) and transmission electron microscope (JEOL JEM 2010F, field emission electron microscope) operated at 200 kV. The BET surface area was evaluated by N_2 adsorption in a constant volume adsorption apparatus (Micrometrics, ASAP 2012). The chemical states of sulfur in the samples were determined from X-ray photoelectron spectroscopy measurements (XPS VG Scientific, ESCALAB 220iXL) using Mg Kα radiation (1253.6 eV). The binding energy calibration was performed using C1s peak in the background as the reference energy (284.6 eV).

2.4. Photocatalytic reaction procedures

The photocatalytic reactions were carried out at room temperature under normal pressure in a closed circulation system using a Hg-arc lamp (350 W) equipped with UV cut off filter ($\lambda \geq 420$ nm). The H_2 evolution was determined in an aqueous solution (100 ml) containing 0.1 g catalyst and 0.1 M Na_2S + 0.02 M Na_2SO_3. The evolved amounts of H_2 were analyzed by gas chromatography (TCD, molecular sieve 5-Å column and Ar carrier). Pt metal-loaded catalysts were prepared by in situ photodeposition method: composite photocatalyst was added in aqueous methanol solution containing a required amount (0.25–2.0 wt%) of H_2PtCl_6 and filtered and then dried in a static oven. Other metal cocatalysts (Pd, Rh and Ru) were also loaded by the photodeposition method to obtain 0.75 wt% loading with aqueous solution of $PdCl_2$, $RhCl_3 \cdot xH_2O$ and $RuCl_3 \cdot xH_2O$.

3. Results and discussion

3.1. Optimization of bulk CdS photocatalysts

We first optimized preparation of CdS alone in order to prepare efficient CdS(bulk)/TiO_2 NBC composite photocatalysts. Fig. 1 shows XRD patterns of CdS samples prepared at various temperatures. As described, CdS sol was prepared by a precipitation method in isopropyl alcohol. The material was heated at 673–1073 K for 1 h under He flow in order to increase

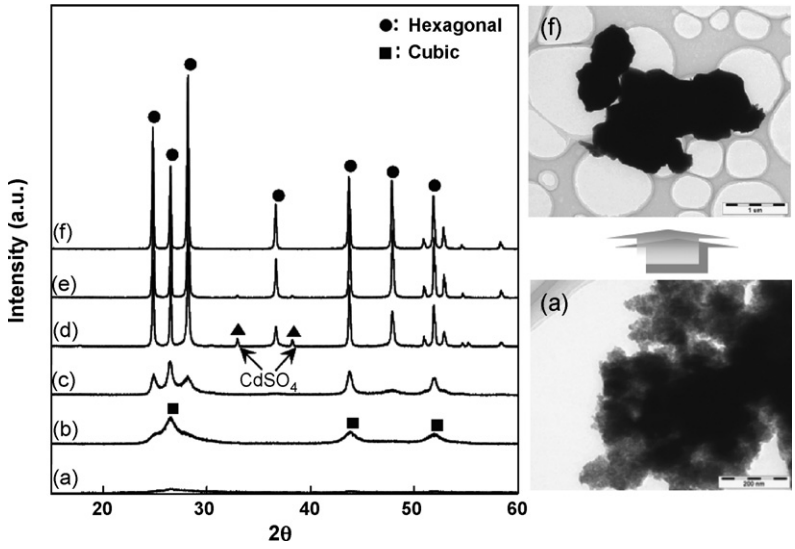

Fig. 1. X-ray diffraction patterns of CdS heated under He flow (μmol s^{-1}) at different temperatures: (a) CdS not heated, (b) CdS-673 K, (c) CdS-773 K, (d) CdS-873 K, (e) CdS-973 K and (f) CdS-1073 K. TEM images of (a and f) show morphologies of the samples (a and f).

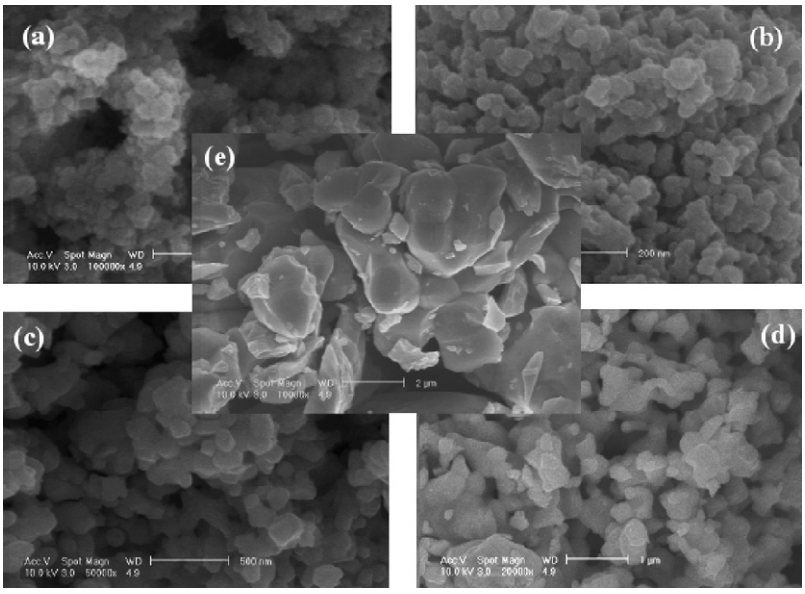

Fig. 2. SEM images of: (a) CdS-673 K, (b) CdS-773 K, (c) CdS-873 K, (d) CdS-973 K and (e) CdS-1073 K. All samples were heat-treated under He flow for 1 h.

the crystallinity. As shown in Fig. 1, the crystallinity of prepared CdS was enhanced according to increase of heat treatment temperature and CdS samples heated above 873 K showed a well-developed hexagonal phase. The high temperature annealing induces the formation of the hexagonal wurtzite phase (Fig. 1), which is known to be the more active phase than the low-temperature, cubic zinc blende phase [16]. In addition, heat treatment could heal surface defects in the crystallites, which are responsible for the energy-wasteful photoelectron–hole recombination. The XRD pattern of the sample prepared at 873 K shows two small peaks of $CdSO_4$ due to the partial oxidation of surface (Fig. 1(d)). This impurity phase can induce a low photocatalytic activity for hydrogen production.

The morphology of CdS particles after heating at the high temperatures was observed by TEM (Fig. 1) and SEM (Fig. 2). The morphology of the untreated sample was agglomerates of nanosized particles with no distinctive morphological feature. Upon annealing at high temperatures, TEM and SEM images showed particle sizes of ca. 1–2 μm.

Fig. 3 shows the UV-diffuse reflection (UV-DR) spectra of CdS samples annealed at various temperatures. The shape and position of absorption edges did not vary much. But, as the annealing temperature increased, the absorption intensity was reduced. All the absorption edges were very sharp except the untreated CdS, which seemed to reflect the poor crystallinity of the sample. The absorption edge also showed a slight red-shift with increase in treatment temperature. This appears to be due the "quantum size effect" of CdS nanoparticle formed at low temperatures.

Shown in Fig. 4 are the correlation curves for evolution rates of H_2, the specific BET surface area, and particle size of CdS photocatalysts with annealing temperatures. The average rate of hydrogen evolution of CdS having high crystallinity (hexagonal wurtzite phase) as a result of heat treatment at the high temperatures was faster than those of cubic zinc blende phases that were not annealed or annealed at lower temperatures. This again seemed to be the effect of CdS crystallinity as previously reported [16]. Thus, there exists a critical annealing temperature (973 K in the present case), at which abrupt changes are observed in the H_2 evolution rates of H_2, the specific BET surface area and the particle size of photocatalysts. These changes are accompanied by the change in the crystal structure of CdS from the cubic zinc blende phase to the hexagonal wurtzite phase. In addition, the high crystallinity of CdS will reduce surface defects in the crystals, which play a role of recombination center of photogenerated electron and hole. Indeed, it was reported that hexagonal wurtzite phase showed the higher oxidation activity of aqueous electrolyte solution containing S^{2-} or SO_3^{2-} than that of cubic zinc blende CdS [17].

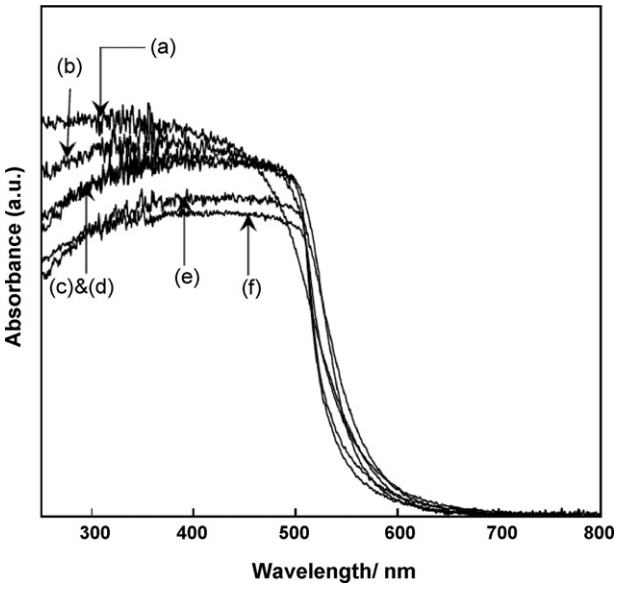

Fig. 3. UV–vis diffuse reflectance spectra of: (a) CdS not heated, (b) CdS-673 K, (c) CdS-773 K, (d) CdS-873 K, (e) CdS-973 K and (f) CdS-1073 K.

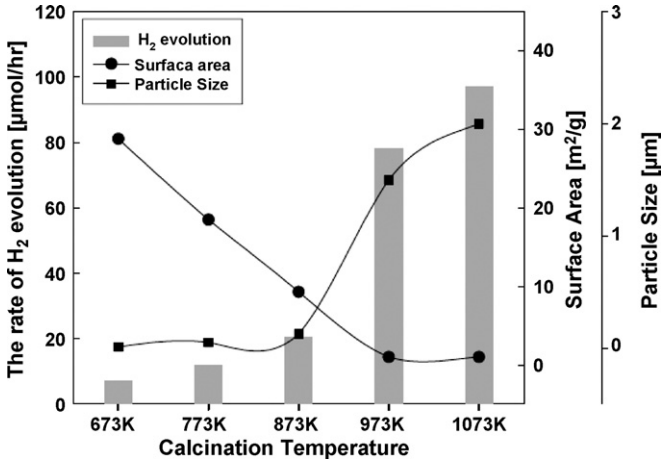

Fig. 4. Correlation curves for evolution rates of H_2, the specific BET surface area and the particle size of photocatalysts with calcination temperatures. All samples were heat-treated at various temperatures under He flow for 1 h.

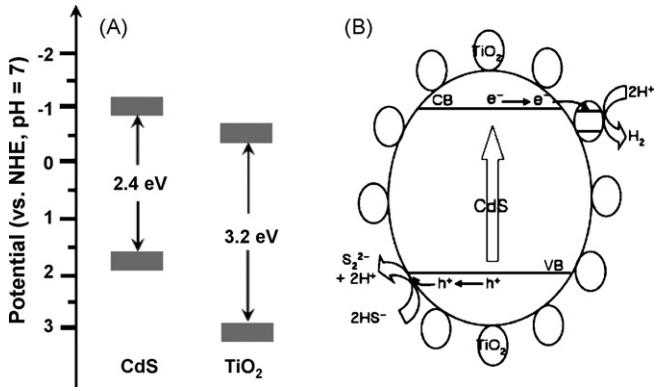

Fig. 5. (A) Conduction band and valence band positions (vs. NHE, pH 7) of CdS and TiO_2. (B) A configuration model consisting of bulky CdS with high crystallinity decorated with nanosized TiO_2 particles.

There was an apparent induction period of 1–2 h before the steady state hydrogen evolution rate was established. This result is in agreement with that of a previous work of Serpone and Borgarello [18]. The surface sulfur species of CdS was analyzed by XPS to investigate the oxidation state on surface of CdS (not shown here). The S2p peaks indicated that CdS-1073 K contained a small peak at ca. 169 eV attributed to SO_4^{2-} as an impurity [16,19]. Generally, CdS can be oxidized to CdO and $CdSO_4$ forming impurity phases and both of them are not active phases for photocatalytic hydrogen generation. Thus, CdO cannot produce H_2 because its position of the conduction band is more positive than the redox potential of H^+/H_2 [20]. $CdSO_4$ is also known to decrease visible light absorption of CdS [21]. This surface oxidation may be responsible for the induction period.

3.2. Optimization of CdS/TiO_2 composite photocatalysts

In our previous work [15], it was reported that CdS(bulk)/TiO_2 composite photocatalyst showed a high photocatalytic activity for hydrogen production from electrolyte solution containing sulfide and sulfite as sacrificial reagents under visible right irradiation ($\lambda \geq 420$ nm). Its activity was much higher than that of single CdS photocatalyst having a high crystallinity, and those of composite photocatalysts of different configurations, i.e. nano-CdS/bulk-TiO_2 or nano-TiO_2/bulk-CdS. The superior activity of the composite photocatalyst is considered to be due to a fast charge separation. Thus, difference in the positions of conduction bands drives photoelectrons generated in bulky CdS upon initial light absorption to surrounding TiO_2 nanoparticles as shown in a schematic model (Fig. 5) [22]. In order for this system to function efficiently, highly crystalline CdS phase appears necessary. To investigate the optimum molar concentration of TiO_2 in CdS(bulk)/TiO_2

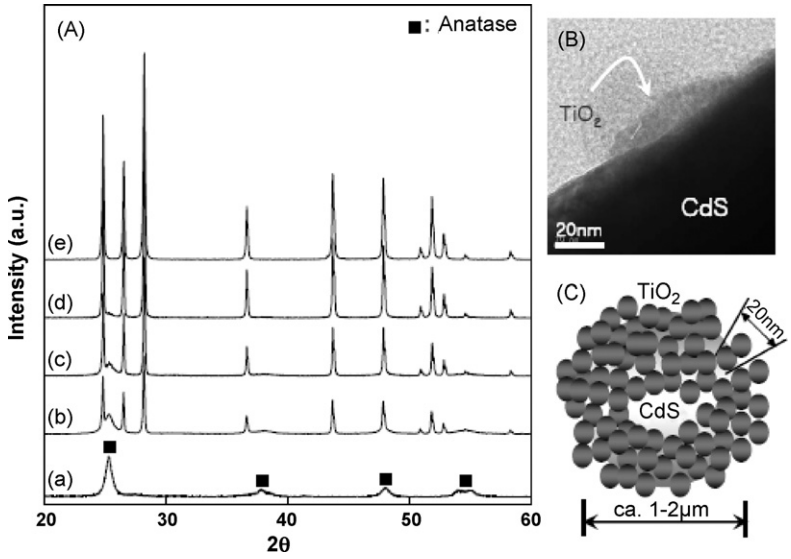

Fig. 6. (A) X-ray diffraction pattern of the samples with different molar ratios of TiO_2 in CdS(bulk)/TiO_2 composite photocatalysts ([TiO_2]/[TiO_2] + [CdS]): (a) 1.0 (TiO_2 only), (b) 0.8, (c) 0.67, (d) 0.33 and (e) 0 (CdS only). All samples were calcined at 673 K for 1 h under air. (B) TEM image of (b) sample. (C) A schematic model of the CdS(bulk)/TiO_2 composite photocatalyst.

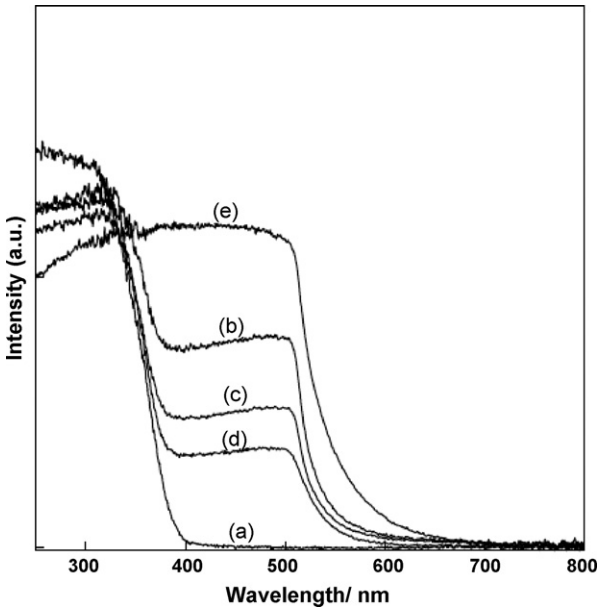

Fig. 7. UV–vis diffuse reflectance spectra of the samples with different molar ratios of TiO_2 in CdS(bulk)/TiO_2 composite photocatalyst ([TiO_2]/[TiO_2] + [CdS]): (a) 1.0 (TiO_2 only), (b) 0.8, (c) 0.67, (d) 0.33 and (e) 0 (CdS only). All samples were calcined at 673 K for 1 h under air.

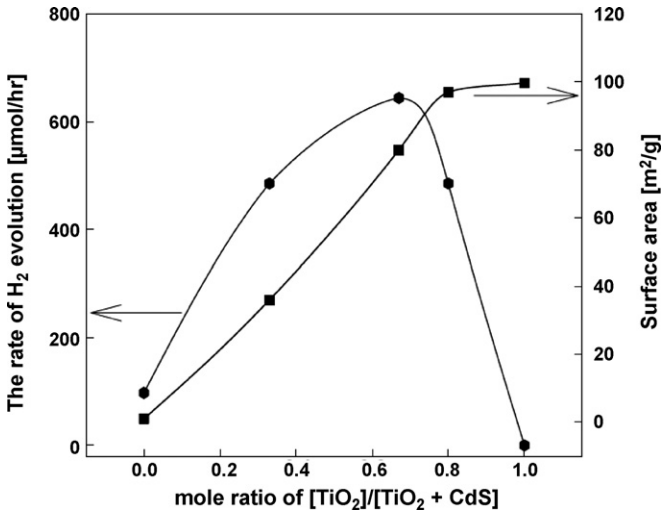

Fig. 8. Correlation curves for evolution rates of H_2 and the specific BET surface area of photocatalysts for catalysts of different [TiO_2]/[TiO_2] + [CdS] ratios: (a) 1.0 (TiO_2 only), (b) 0.8, (c) 0.67, (d) 0.33 and (e) 0 (CdS only). All samples were calcined at 673 K for 1 h under air flow.

composite photocatalyst for hydrogen production, we changed the molar ratio of TiO_2 to CdS. Fig. 6(A) shows XRD patterns of the samples prepared with different molar concentrations of TiO_2 in CdS(bulk)/TiO_2 composite photocatalysts. When the mole ratio of TiO_2 to CdS increased, TiO_2 anatase phase became clearer. The pure CdS showed well-developed hexagonal phase, whereas the TiO_2 phase was anatase both in single and composite photocatalysts. The morphology of CdS/TiO_2 composite photocatalysts was observed by TEM as shown in Fig. 6(B). In CdS(bulk)/TiO_2, CdS particles of ca. 1–2 μm was decorated with TiO_2 nanoparticles of ca. 10–20 nm. This clearly defined geometry of nanoparticles in contact with a large bulk particle is schematically shown in Fig. 6(C). Note that TiO_2 particles would form random multiple particle layers on bulk CdS surface as discussed below.

The UV-diffuse reflectance (DR) spectra for these catalysts are shown in Fig. 7. The bulky CdS photocatalyst showed a sharp edge at 570 nm, while TiO_2 showed an edge at 390 nm. The spectra of all CdS(bulk)/TiO_2 composite photocatalysts showed a combination of these two spectra, although the addition of TiO_2 led to a blue-shift of the absorption edge of CdS to 550 nm in composite photocatalysts. This is in agreement with the previous report by Kisch et al. that the band gap of CdS employed in composite photocatalysts is shifted by an electronic semiconductor-support interaction (SEMSI) [23,24].

Fig. 8 shows the effect of the mole ratio of [TiO_2]/[TiO_2] + [CdS] for hydrogen production from an aqueous solution containing 0.1 M Na_2S and 0.02 M Na_2SO_3 as sacrificial reagents under visible light irradiation ($\lambda \geq 420$ nm). The optimum molar concentration of TiO_2 in CdS(bulk)/TiO_2 that showed the highest activity for H_2 evolution was determined to be 0.67 as shown in Fig. 8. Thus, an optimum content of nanosized TiO_2 particles decorating bulky CdS exists that induces the highest rate of hydrogen production under visible light ($\lambda \geq 420$ nm) irradiation from water containing sulfide and sulfite ions as hole scavengers. Thus, the coverage of TiO_2 nanoparticles decorating bulky CdS is needed for effective and fast charge separation of photogenerated electrons and holes, and to increase the photocatalytic activity. But too high a coverage would shade CdS surface responsible for the visible light absorption. This optimum content is rather high at [TiO_2]/[TiO_2] + [CdS] mole ratio of 0.67. This corresponds to more than 10 times as much as the amount needed to cover 2 μm CdS particles with a complete monolayer of 20 nm TiO_2 particles. This indicates that TiO_2 nanoparticles tend to be deposited forming random multilayers over bulky CdS rather than the layer-by-layer deposition.

3.3. *Effect of calcination of CdS(bulk)/TiO_2 composite photocatalysts*

TiO_2 nanoparticles synthesized in this work by the sol–gel method are in contact with the surface of bulky CdS. The effect of heat treatment of CdS alone has been discussed in Section 3.1. In order to investigate the effect of heat treatment of TiO_2 in these composite photocatalysts, we varied the calcination temperature of CdS(bulk)/TiO_2 composite photocatalyst in air flow.

Fig. 9 shows XRD patterns of CdS(bulk)/TiO_2 powders calcined at various temperatures to increase the crystallinity of TiO_2 nanoparticles in CdS(bulk)/TiO_2 composite. The samples calcined at RT and 573 K did not show the main peak of the anatase TiO_2 phase. But, the XRD patterns of CdS(bulk)/TiO_2 composite calcined at 673–873 K showed the anatase TiO_2 phase. When calcination temperature was increased from 673 to 773 K, (1 0 0) peak of anatase phase became clearer, indicating that TiO_2 nanoparticles calcined at higher temperatures had better crystallinity.

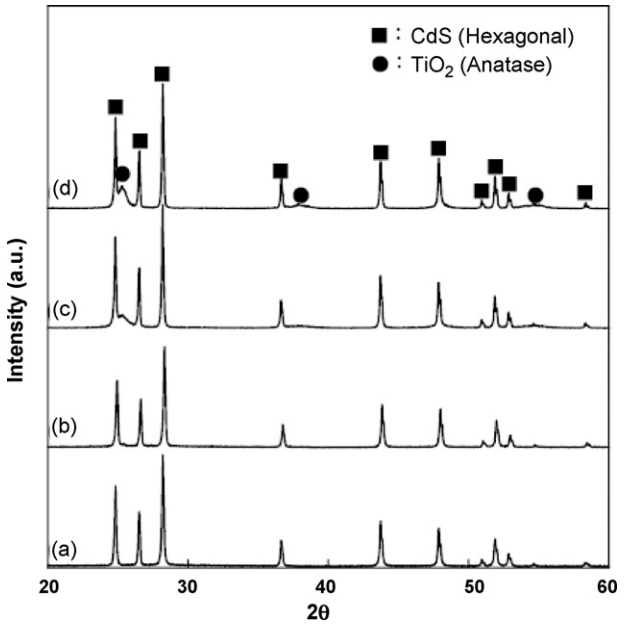

Fig. 9. X-ray diffraction pattern of composite photocatalysts prepared at various temperatures for 1 h under air flow: (a) RT, (b) 573 K, (c) 673 K and (d) 773 K. The molar ratio of $[TiO_2]/([TiO_2]+[CdS])$ was 0.67.

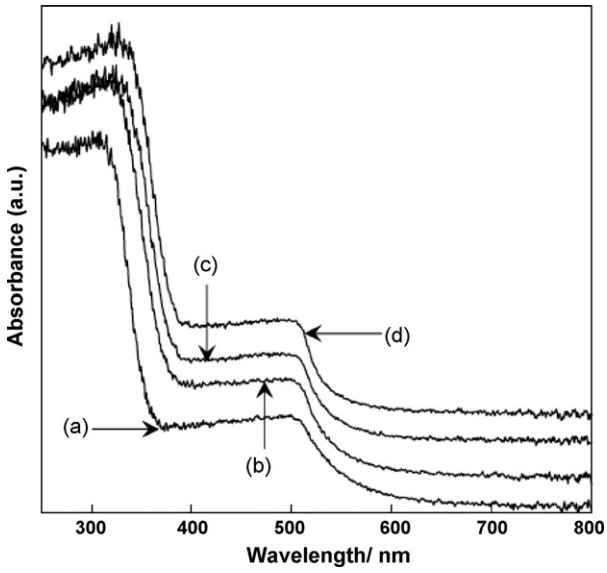

Fig. 10. UV–vis diffuse reflectance spectra of composite photocatalysts prepared at various temperatures for 1 h under air flow: (a) RT, (b) 573 K, (c) 673 K and (d) 773 K. The molar ratio of $[TiO_2]/([TiO_2]+[CdS])$ was 0.67.

Fig. 10 shows the UV–vis diffuse reflection spectra of CdS(bulk)/TiO_2 samples calcined at RT ~ 773 K for 1 h. Overall, CdS(bulk)/TiO_2 composites showed the same UV-DR spectra that showed characteristics of both CdS and TiO_2(bulk) just like a physical mixture of two compounds. As the calcination temperature increased, the absorption edge at the lower wavelength due to TiO_2 showed a systematic red-shift, indicating the growth of TiO_2 crystals with calcination temperatures.

Fig. 11 shows TEM images of CdS(bulk)/TiO_2 samples calcined at 573–773 K for 1 h. The morphology of TiO_2 in the CdS(bulk)/TiO_2 sample calcined at 573 K seemed to be an amorphous phase. The particle shape of TiO_2 decorating bulky CdS became clearer forming ca. 20 nm particles at increased calcination temperatures. This result is consistent with that of XRD pattern.

Fig. 12 shows dependence of the evolution rate of H_2, the specific BET surface area and the particle size of photocatalysts on the calcination temperature. At three different calcination temperatures, there was a large variation in specific BET surface area and particle size of TiO_2 by XRD data and TEM images. Yet, the variation in the rate of H_2 evolution was very small (<10%). The variation is much smaller than that observed for different mole ratios of CdS nanoparticle to bulky TiO_2 shown in Fig. 8 (ca. 6-fold variation) and for different annealing temperatures of CdS (ca. 10-fold variation). In CdS(bulk)/TiO_2 composite photocatalysts, CdS is the component that absorbs visible light and generates photoelectrons and holes. Annealing of CdS particle could heal surface defects in the crystallites, which are responsible for the energy-wasteful photoelectron–hole recombination and increase its photocatalytic activity. In contrast, TiO_2 in CdS/TiO_2 composite photocatalyst is supposed to play a role of electron transfer medium rather than generation of photoelectrons and holes. Still, the crystallinity and morphology of TiO_2 particles on CdS(bulk) may affect the process of electron injection from CdS to TiO_2, and electron migration in TiO_2. The observed insignificant effect of TiO_2 annealing suggests that these rates in TiO_2 are less important for the overall rates of the photocatalytic reaction relative to rates of steps occurring in CdS.

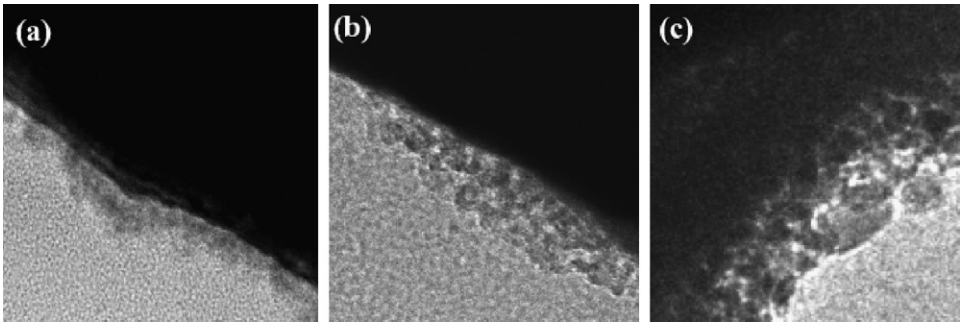

Fig. 11. TEM images of composite photocatalysts prepared at various temperatures for 1 h under air flow: (a) 573 K, (b) 673 K and (c) 773 K. The molar ratio of $[TiO_2]/([TiO_2]+[CdS])$ was 0.67.

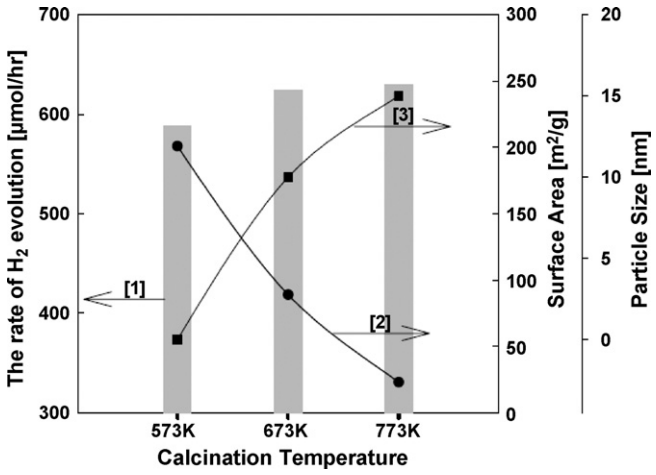

Fig. 12. Dependence of the evolution rate of H_2, the specific BET surface area and the particle size of photocatalysts on calcination temperature. The molar ratio of $[TiO_2]/([TiO_2]+[CdS])$ was 0.67. All samples were heat-treated at various temperatures under He flow for 1 h. Particle size was determined by TEM images.

3.4. Effect of novel metal loading on CdS(bulk)/TiO_2 composite photocatalyst

Hydrogen production depended on the nature of noble metals loaded on the composite photocatalyst. Sathish et al. [25] reported that there is a direct correlation between the rate of hydrogen evolution and properties of such metals, i.e. redox potential, work function and metal–hydrogen bond strength. Thus, Pt metal with higher redox potential, work function and lower metal hydrogen bond strength was found to be favorable for hydrogen evolution activity.

Fig. 13 shows the photocatalytic activity for hydrogen production according to the nature of noble metals loaded on CdS(bulk)/TiO_2 composite. The amount of hydrogen gas evolved under visible light irradiation increased in the following sequence for noble metals loaded on CdS(bulk)/TiO_2 samples: Pt (640 μmol/h for H_2) > Rh (459 μmol/h for H_2) > Pd

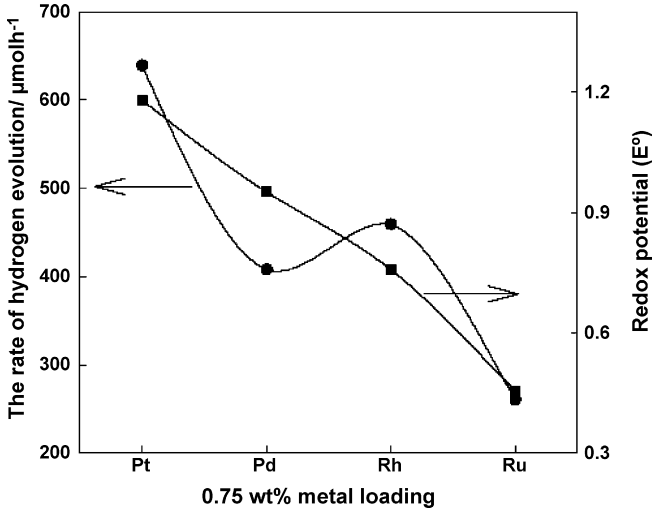

Fig. 13. A correlation between the rates of H_2 evolution and redox potential for different noble metals. Metal loading: 0.75 wt%.

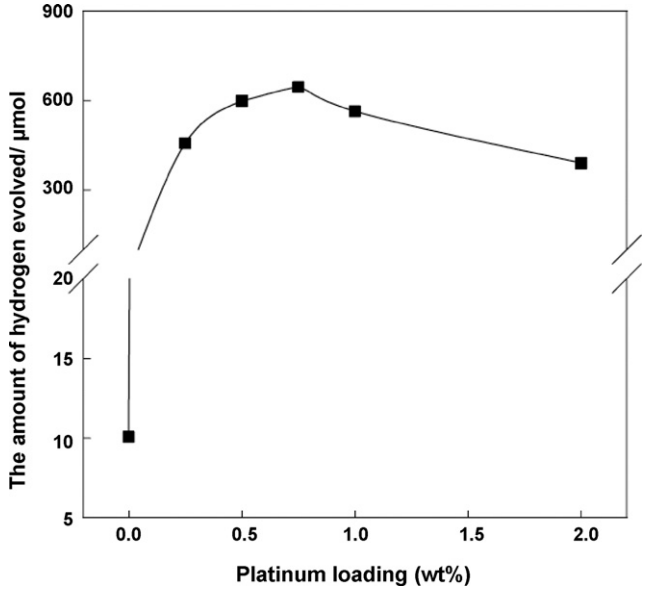

Fig. 14. Effects of the amount of platinum loaded on CdS(bulk)/TiO_2 on hydrogen evolution rates.

(408 μmol/h for H_2) > Ru (261 μmol/h for H_2). There exists significant difference for hydrogen production among different cocatalysts. Platinum was the best cocatalyst among them to produce hydrogen over CdS(bulk)/TiO_2 composite photocatalyst. Yet, the correlation of the photocatalytic activity with redox potential of the cocatalysts was not obvious as shown in Fig. 13.

We investigated the dependence of the photocatalytic activity on the amount of Pt loading on CdS(bulk)/TiO_2 composite. As shown in Fig. 14, the photocatalytic activity increased with the amount of Pt metal up to 0.75 wt% and then decreased gradually with further increase of the amount of Pt loading, showing a maximum activity at 0.75 wt%. Thus, it was necessary to have an optimum level of Pt loading on CdS(bulk)/TiO_2 for efficient hydrogen production.

4. Conclusions

From the results of optimization of composite photocatalysts, it can be concluded that the crystallinity of CdS is more important than that of TiO_2 and that the formation of CdS(bulk)/TiO_2 composite photocatalyst is more effective strategy than single CdS photocatalyst to acquire an active photocatalyst. The optimum molar concentration of TiO_2 in CdS(bulk)/TiO_2 composite photocatalyst that showed the highest activity for H_2 evolution was determined to be 0.67. The photocatalytic activity increased with the amount of Pt metal cocatalyst showing the maximum activity at 0.75 wt% and decreased gradually with further increase of the amount of Pt loaded. There exists a significant difference in hydrogen production activity among different cocatalysts (Pt, Pd, Rh and Ru).

Acknowledgments

This work has been supported by Hydrogen Energy Center (a Frontier Research Program of KOSEF) and BK-21 program.

References

[1] A. Kudo, Catal. Surv. Asia 7 (2003) 31.
[2] K. Domen, M. Hara, J.N. Kondo, T. Takata, A. Kudo, H. Kobayashi, Y. Inoue, Korean J. Chem. Eng. 18 (2001) 862.
[3] H.G. Kim, H.B. Pramod, W. Choi, J.S. Lee, Angew. Chem. Int. Ed. 44 (2005) 4585.
[4] H. Kato, K. Asakura, A. Kudo, J. Am. Chem. Soc. 125 (2003) 3082.
[5] H.G. Kim, D.W. Hwang, J.S. Lee, J. Am. Chem. Soc. 126 (2004) 8912.
[6] H. Fujii, M. Ohtaki, K. Eguchi, H. Arai, J. Mol. Catal. A 129 (1998) 61.
[7] W.W. So, K.J. Kim, S.J. Moon, Int. J. Hydrogen Energy 29 (2004) 229.
[8] N. Buhler, K. Meier, J. Reber, J. Phys. Chem. 88 (1984) 3261.
[9] A.J. Frank, K. Honda, J. Phys. Chem. 86 (1982) 1933.
[10] D. Meissner, R. Memming, B. Kastening, J. Phys. Chem. 92 (1988) 3476.
[11] A. Sobczynski, A.J. Bard, A. Campion, M.A. Fox, T. Mallouk, S.E. Webber, J.M. White, J. Phys. Chem. 91 (1987) 3316.
[12] L. Spanhel, H. Weller, A. Henglein, J. Am. Chem. Soc. 109 (1987) 6632.
[13] T. Kida, G. Guan, A. Yoshida, Chem. Phys. Lett. 371 (2003) 563.
[14] W. Shangguan, A. Yoshida, J. Phys. Chem. 106 (2002) 12227.
[15] J.S. Jang, W. Li, S.H. Oh, J.S. Lee, Chem. Phys. Lett. 425 (2006) 278.
[16] M. Matsumura, S. Furukawa, Y. Saho, H. Tsubomura, J. Phys. Chem. 89 (1985) 1328.
[17] Y. Nakaoka, Y. Nosaka, J. Phys. Chem. 99 (1995) 9893.
[18] N. Serpone, E. Borgarello, Inorg. Chim. Acta 90 (1984) 191.
[19] M. Lichtensteiger, C. Webb, J. Appl. Phys. 54 (1983) 2127.
[20] M. Fujii, T. Kawai, S. Kawai, Chem. Phys. Lett. 106 (1984) 517.
[21] H. Fujii, M. Ohtaki, K. Eguchi, H. Arai, J. Mol. Catal. A: Chem. 129 (1998) 6.
[22] R. Vogel, P. Hoyer, H. Weller, J. Phys. Chem. 98 (1994) 3183.
[23] H. Weib, A. Fernandez, H. Kisch, Angew. Chem. Int. Ed. 40 (2001) 3825.
[24] H. Kisch, H. Weib, Adv. Funct. Mater. 12 (2002) 483.
[25] M. Sathish, B. Viswanathan, R.P. Viswanath, Int. J. Hydrogen Energy 31 (7) (2006) 891.